Effects of radio-frequency current on spin-transfer-torque-induced dynamics

S. H. Florez,* J. A. Katine, M. Carey, L. Folks, O. Ozatay, and B. D. Terris
San Jose Research Center, Hitachi Global Storage Technologies, 3403 Yerba Buena Road, San Jose, California 95135, USA
(Received 27 March 2008; revised manuscript received 1 October 2008; published 7 November 2008)

The impact of radio-frequency (rf) currents on the direct current (dc)-driven switching dynamics in current-perpendicular-to-plane nanoscale spin valves is demonstrated. The rf currents can dramatically alter the dc-driven free layer magnetization reversal dynamics as well as the dc switching level. The effects occur when the frequency of the rf current is tuned to a frequency range around the dc-driven magnetization precession frequencies. For these frequencies, interactions between the dc-driven precession and the injected rf induce frequency locking and frequency pulling effects that lead to a measurable dependence of the critical switching current on the frequency of the injected rf. Based on macrospin simulations, including dc as well as rf spin torque currents, we explain the origin of the observed effects.

DOI: 10.1103/PhysRevB.78.184403 PACS number(s): 75.60.Jk, 75.70.Cn, 73.40.−c

I. INTRODUCTION

Direct electrical currents, via the spin-transfer torque (STT), can excite a broad variety of magnetization dynamics including reversal and steady-state precessional states in current-perpendicular-to-plane spin valves.[1,2] These precessional dynamics, stabilized by the opposing effects of the STT and the damping torque, in addition to being of great scientific interest have important implications for the development of new radio-frequency (rf) devices. While prior studies focused on the dynamics in the nonhysteretic regime, it has also been recognized that precessional dynamics can exist in the hysteretic regime.[3–7] In particular, we concentrate on the *preswitching* (PS) precessional modes, arising for direct currents above the threshold value for the development of dynamic instabilities I_t,[4,6] yet below the critical current for switching I_c. These modes are of great interest as they drive the switching dynamics and control of switching is key to potential memory and logic applications.

In this work we investigate the PS dynamical regime as well as the effects of additional rf currents on the PS and switching modes. These PS modes are found to interact with applied rf currents having frequencies in the range of the *dc-only* driven modes and under certain conditions are found to frequency lock. In contrast to previous frequency locking experiments,[8–10] by looking at these effects in the PS regime, we find a measurable dependence of the dc switching threshold on the external rf frequency f_{inj}. In the locking range the rf appears to have a stabilizing effect which hinders switching, however, at frequencies just below this range, we find a measurable reduction in I_c.[11] In this work, by studying the behavior of this system in frequency domain and through macrospin simulations (using the Landau-Lifshitz-Gilbert equation with Slonczewski type spin-transfer torque[2]) we provide a description of the magnetization dynamics originating from the interaction between the dc-driven switching modes and the applied rf current. The results show good qualitative agreement with our experimental data.

II. EXPERIMENT

The samples are 50×100 nm^2 hexagonal pillars comprised of an IrMn pinning layer, an antiparallel (AP)-coupled bilayer $Co_{50}Fe_{50}$(25 Å)/Ru(8 Å)/$Co_{50}Fe_{50}$(25 Å) as the fixed layer, a 40 Å Cu spacer, and 35 Å $Ni_{92}Fe_8$ as the free layer (FL). All observed current-induced magnetic excitations occur in the FL. In our system of reference negative currents or positive fields (below ~1 kOe) stabilize the AP magnetization state. Here we present results from a single element, selected due to its comparatively high power PS modes even in the absence of an applied external field H_{app}. This is likely due to the significant dipolar field H_{dip} ~170 Oe, at the free layer (estimated from the field hysteresis curve offset), despite the use of AP-coupled pinning layers. We point out, however, that variations from one element to another are observed and furthermore, PS dynamics are not detectable for all pillars. Nevertheless, qualitatively similar results were obtained for all samples for which similar amplitude PS modes were observed.

Experiments were performed in a variable-temperature *Desert Cryogenics* probe station equipped with a superconducting magnet for applying in-plane magnetic fields. Contact to the pillar was made through high-frequency ($<$40 GHz) probes connected to the (rf+dc) mixing port of a broadband bias tee. The inductive port of the bias tee was used for low-frequency dynamic resistance measurements using a lock-in amplifier, while the capacitive side was attached to a +44 dB amplifier connected to a spectrum analyzer. While the sample stage was held at 4.2 K, the true sample temperature, when injecting direct currents I^{dc} on the order of 1 mA, was estimated to be approximately 25 K due to Joule heating (estimated from a comparison of measurements of dV/dI vs I^{dc} and dV/dI vs temperature). All experiments were performed at low temperatures in order to minimize thermal fluctuations. Calibration of the electrical setup was carried out by measuring the temperature-dependent Johnson noise from 50 Ohm test resistors and a network analyzer was used to measure the complex and frequency dependent impedance Z_0 of the sample, which was then used to estimate the amplitude of the injected rf current.

III. RESULTS AND DISCUSSION

The macrospin model predicts the onset of subcritical current driven stable precessional dynamics around the average

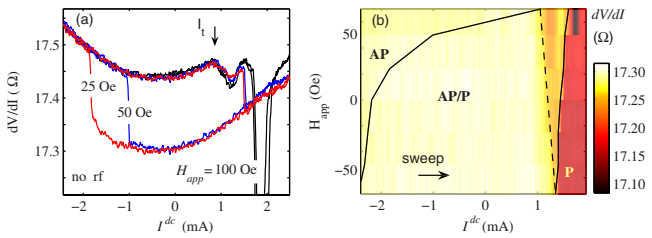

FIG. 1. (Color online) (a) dV/dI vs I^{dc} for current-induced switching loops taken at H_{app}=25, 50, and 100 Oe, and I_t marked by arrow. (b) (I^{dc},H_{app}) phase diagram for hysteretic region with color scale representing dV/dI.

dipolar field for currents above a threshold value I_t, for which the STT balances the damping torque. As I^{dc} increases, the orbits are predicted to expand while precession frequencies decrease.[5,6] Experimentally, we identify potential regions of STT-induced dynamic instabilities in the FL magnetization as anomalies in dV/dI. Figure 1(a) illustrates this for current sweeps taken at H_{app}=25, 50, and 100 Oe, where the field is applied a few degrees off the easy-axis direction. We concentrate mainly on the STT magnetization dynamics prior to the AP to P transition, occurring approximately at −560 Oe at I^{dc}=0 (loop not shown) and 1.45 mA at H_{app} =0.

For currents below the switching value, yet above the instability threshold current I_t, anomalies, appearing as small dips for H_{app}=25,50 Oe (hysteretic) and larger dips for H_{app}=100 Oe (nonhysteretic) in Fig. 1(a), reveal strong microwave activity. Shown in Fig. 1(b) is a phase diagram where the color scale represents dV/dI for I^{dc} swept from negative to positive values and the continuous lines show the switching boundaries obtained for current sweeps in both directions. The PS regime appears as a narrow area on the right side of the dashed line and to the left of the P region. Low positive fields (<100 Oe) that oppose STT yet sustain hysteretic behavior, stabilize and strengthen these precessional states over a wider I^{dc} range, as can be seen through the widening of the PS regime. Similar PS dynamics corresponding to the P to AP transition were also detected for low negative values of applied field.

Examples of power spectral density (PSD) data measured at low temperature and in the PS range are shown in Fig. 2(a). The background noise spectra in the AP state and with I^{dc}=0 have been subtracted from each curve. As I^{dc} increases

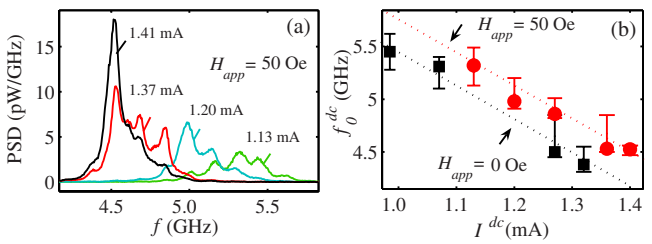

FIG. 2. (Color online) (a) PSD measured at H_{app}=50 Oe for I^{dc} values below the switching value. The PSD measured with I^{dc}=0 has been subtracted. (b) f_0^{dc} vs I^{dc} for H_{app}=0 (squares) and 50 Oe (circles) [symbols at peak value, bar denotes full width at half maximum span].

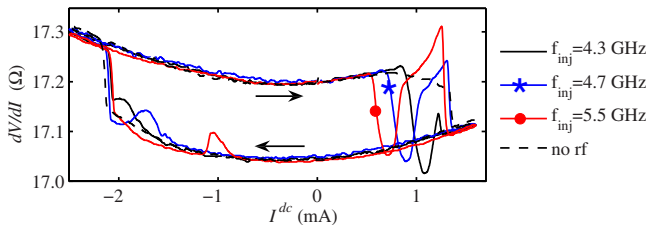

FIG. 3. (Color online) dV/dI vs current-induced switching loops for H_{app}=0 with no rf (dashed) and injected rf (continuous) with f_{inj}=4.3, 4.7, and 5.5 GHz.

in the PS range, the precessional frequencies decrease and we label the frequencies in this range as the *dc-driven PS precessional frequencies* f_0^{dc}. For H_{app}=0, the peak frequencies in this range vary roughly from 5.5 to 4.2 GHz for I^{dc} ranging from ~1–1.4 mA. The emitted power rises with increasing I^{dc}, as f_0^{dc} drops to a minimum $(f_0^{dc})^{min}$, in agreement with the macrospin model. Somewhat higher currents lead to FL magnetization reversal as the PS precessional modes disappear. In Fig. 2(b) we plot the measured f_0^{dc} vs I^{dc} for H_{app}=0 and 50 Oe, showing the peak frequencies decrease as the current rises toward the switching value I_c. Extrapolation of these data through I_c suggests that the minimum resonance frequency $(f_0^{dc})^{min}$, approaching reversal and for H_{app}=0 is near 4.2 GHz. Following Kiselev *et al.*,[3] we make a macrospin estimation of the precession and misalignment angles (between the pinned layer and the FL) by assuming small-angle precession and measuring the total integrated power in the first and second harmonics. While this approximation may be imprecise, in view of the highly non-Lorentzian spectra, it provides a useful indication of the behavior of the precessional dynamics as I^{dc} is ramped. For low applied field values between $0<H_{app}<100$ Oe and I^{dc} increasing from 1 to 1.4 mA, we find precessional angles increasing roughly from 10° to 30°. This type of incoherent behavior, with linewidths on the order of ~500 MHz, has been observed in micromagnetic modeling[12] and can be understood from the spatially nonuniform local demagnetizing fields at the edges of the spin-valve device. However, the ripple structure on the data may be a measurement artifact (from reflections along the line) that is not completely eliminated by the background noise subtraction.

The effect of adding a rf current I^{rf} to I^{dc} on the FL STT dynamics can be seen from the dV/dI vs current hysteresis loops shown in Fig. 3. This figure includes data for the no rf case (dashed line) and for three different injected frequencies f_{inj}=4.3, 4.7, and 5.5 GHz, all selected to be in the f_0^{dc} range. In all cases, a power of −15 dBm was applied at the signal generator, resulting in $(I^{rf})^{rms}\sim 1$ mA. The anomalies (dips or peaks) appearing before the AP to P (or P to AP) transition are caused by interactions between I^{rf} and the I^{dc} driven precession resulting in changes in the FL magnetization trajectory and consequently in the magnetoresistance. Focusing on the AP to P preswitching range, note that with decreasing f_{inj}, the I^{dc} level at which the anomaly occurs increases thereby following the f_0^{dc} *redshift* induced by increasing I^{dc}. We have observed this type of behavior in samples with two different FL materials and with PS precessional frequencies in distinct

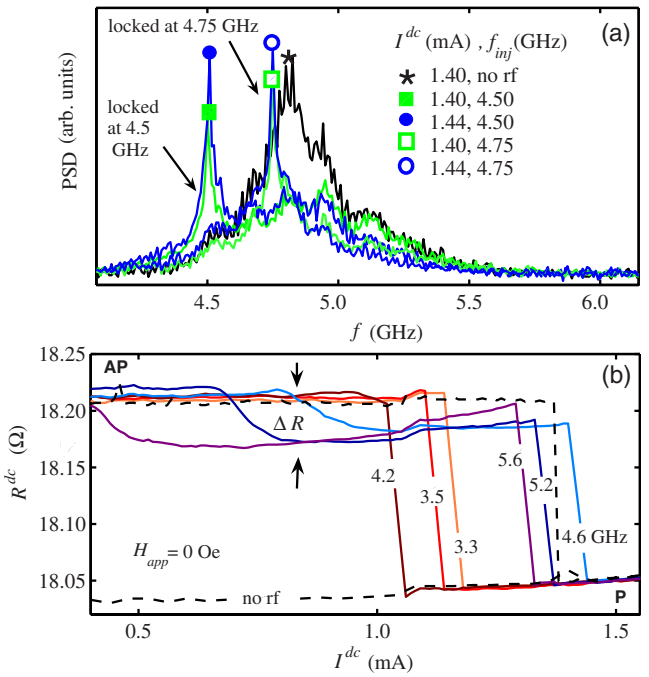

FIG. 4. (Color online) (a) Comparison of the PSD with (circles, squares) and without (star) rf for I^{dc} in the PS range and H_{app} =25 Oe, showing frequency locking for f_{inj}=4.5 and 4.75 GHz. (b) R^{dc} vs I^{dc} for currents just below I_c corresponding to the AP to P switch and for several values of injected rf frequencies. The dashed line shows the no rf case.

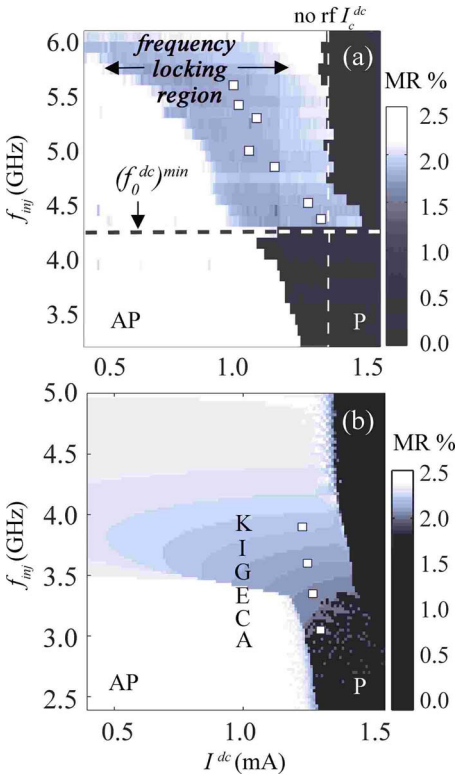

FIG. 5. (Color online) (a) Measured (I^{dc},f_{inj}) phase map obtained at H_{app}=0 with R^{dc} represented through gray scale. The white squares show the locations of the measured f_0^{dc}. (b) Macrospin model of the (I^{dc},f_{inj}) phase map, with grayscale representing the final-state MR. The white squares show the locations of the simulated f_0^{dc}.

frequency ranges,[11] from which we infer a general behavior.

To elucidate the effects of the rf current on the FL dynamics, we studied the changes in the frequency domain behavior induced by adding I^{rf} to I^{dc}. In this case the setup was modified by adding a 3–7 GHz power splitter to inject and measure high-frequency signals to and from the sample. Results suggest that for injected frequencies in the range of f_0^{dc} and currents in the PS regime, partial frequency locking between the dc-driven precession and the external rf signal, as shown in Fig. 4(a), can occur. For these experiments, the power was limited to −23 dBm to avoid saturating the amplifier. Low applied fields of less than 50 Oe were applied to enhance the signal. Figure 4(a) illustrates the partial frequency locking of the dc-driven precessional modes with the external rf, observed at I^{dc}=1.40 and 1.44 mA, with and without external rf (after subtracting the external rf signal). While the peak frequency in the spectrum for I^{rf}=0 is at 4.8 GHz, applying I^{rf} with f_{inj} at 4.5 or 4.75 GHz narrows the signal and shifts the measured power to the f_{inj} value. As expected, locking only occurs when I^{rf} is applied at a frequency at which the dc-driven mode also has significant power.

Additional insight can be extracted from dc resistance R^{dc} measurements, which differ from the dV/dI measurements in this non-Ohmic device. As shown in Fig. 4(b), for f_{inj} in the f_0^{dc} range, a reversible plateau forms in the PS current range, with a ΔR of approximately 0.05 Ω. As was the case for the rf-induced anomalies in dV/dI, the effect appears at lower values of I^{dc} for higher injected frequencies. The R_{dc} data also show that for f_{inj} below ~4.2 GHz, the plateau does not form and I_c drops as the f_{inj} increases toward this value.

Overall, our measurements suggest that the (I^{dc},f_{inj}) values for which frequency locking occurs coincide with the appearance of both the anomalies in dV/dI and the formation of the plateau in the dc resistance. In these measurements, as I^{dc} is ramped, the corresponding f_0^{dc} drops and frequency locking can only occur for I^{dc} in a range such that f_0^{dc} is within the locking range of f_{inj}. In this range, it appears that the frequency locking influences the FL magnetization dynamics in a way that generates these effects in dV/dI and R_{dc}. We point out, however, that frequency locking is also expected to produce a dc rectification voltage,[8,9] and this effect may also contribute to the dc level in the plateau. As is expected, it was also verified that the extent of the I^{dc} range over which the plateau in R_{dc} forms increases with the injected rf power. Lastly, for f_{inj} in a range below $(f_0^{dc})^{min}$, both dV/dI (as shown in Ref. 11) and R_{dc} confirm a reduction in I_c.

In Fig. 5(a) we plot R^{dc} in color scale for values near the AP to P transition, thereby generating an (I^{dc},f_{inj}) phase diagram. The diagram shows the reduction trend in I_c as f_{inj} increases in a range below ~4.2 GHz. This reduction in I_c is well above the sweep-to-sweep variation. For this specific sample, we estimate the magnitude of the variations in I_c by measuring ~80 loops with f_{inj}=4 and 5 GHz. We account for a slight frequency dependence of the sample impedance by applying at each f_{inj} the power required to pass an equal

magnitude $(I^{rf})^{rms}=1$ mA through the sample. The difference between the average switching currents $\langle I_c^{4\ GHz}\rangle$ and $\langle I_c^{5\ GHz}\rangle$ is greater than 15%. The standard deviations are below 3%. Also in Fig. 5(a), for f_{inj} in the f_0^{dc} range, we identify the plateau, labeled as the *frequency locking region*, as well as an increase in I_c, for f_{inj} above $(f_0^{dc})^{min}$. The open squares show the approximate locations of the $f_0^{dc}(I^{dc})$ peak resonances, which are centered in the locking region as expected.

IV. MACROSPIN SIMULATIONS

The rf-driven effects were modeled through macrospin simulations based on the Landau-Lifshitz-Gilbert equation using Slonzcewski[2] type spin torque. Simulation parameters include saturation magnetizations of $M_s^{pinned}=1100$ emu/cm^3 and $M_s^{free}=810$ emu/cm^3 for the pinned and FL layers, respectively, a spin polarization of $P=0.27$ and a damping factor of $\alpha=0.025$. We also include a uniaxial in-plane FL anisotropy field of 300 Oe, a 200 Oe dipolar field from the fixed layer acting on the FL, and 100 Oe external field (applied along the easy axis to ensure an AP initial condition). Qualitatively speaking, the results are not sensitive to small changes in the simulation parameters and furthermore no effort was made to attain numerical agreement between the simulated and experimental frequencies.

We compared simulation results in time and frequency domains for the cases of $I^{rf}=0$ and $I^{rf}\neq 0$. For an initial AP configuration and no rf, switching for $I^{dc}>1.4$ mA within a 10 ns window was observed. Lower I^{dc} resulted in PS persistent precessional dynamics in which case the calculated Fourier spectral density of the in-plane component of the magnetization along the short axis $M_y(t)$ dropped roughly from 4 to 3 GHz as the current increased from 1.2 to 1.3 mA.

After including the effects of I^{rf} in the macrospin simulation we generated a (I^{dc},f_{inj}) phase diagram obtained by plotting the magnetoresistance (MR) (average value for the final 2 ns of a 20 ns simulation window, normalized to the experimentally obtained MR amplitude) as a function of I^{dc} and f_{inj}. The resulting diagram obtained for $T=0$ and $(I^{rf})^{rms}=1$ mA, to match the experimental I^{rf} amplitude, is shown in Fig. 5(b). The light/dark areas correspond to high/low MR states while the white squares represent the numerically obtained dc-only driven precessional frequencies at several values of I^{dc}.

Qualitatively, the simulations reproduce most of the features of the experimentally obtained map. The switching boundary shows a reduction in I_c for f_{inj} close to the numerically obtained f_0^{dc} for I^{dc} near the switching boundary (3 GHz at 1.3 mA). At slightly higher $f_{inj}\sim 3.5$ GHz, I_c reaches a maximum, and a slow decay follows as f_{inj} continues to increase above 3.5 GHz. Additionally, for f_{inj} in the f_0^{dc} range, and $I^{dc}<I_c$, a drop in the MR with respect to the AP state (regions G, I, K), resembling the drop in MR obtained experimentally in the frequency locking region, is also obtained.

As the macrospin simulations do not include the Oersted field from I^{dc+rf}, we conclude that the rf-induced changes on the magnetization trajectory originate mainly from STT. However, rf *magnetic-field*-induced reductions in switching fields have also been observed[13,14] and it is possible that this effect plays a role in our experiment as well.

The Fourier transform spectrum of the M_y component at different points of the simulated phase diagram shows that the nonlinearity of the system mixes the dc-driven modes and the injected rf and intermodulation products appear in the spectrum, in addition to the components at f_{inj} and f_0^{dc}. As the separation between the latter two frequencies, also known as the *detuning range*, is varied, the system follows the typical behavior of an autonomous oscillator under weak external action.[15] For small detuning ranges, there is a frequency locking regime for which the dc-driven precession synchronizes to the external rf. For somewhat larger detuning ranges, the system enters a frequency pulling regime, for which there are intermittent periods of time with synchronized behavior. For increasingly larger detuning ranges there is a progressive reduction in the duration of the periods of time with synchronized behavior.

The simulations show that in the region of reduced MR [G, I, K in Fig. 5(b)], the dc-driven precession fully synchronizes to the external rf. In this region of the phase diagram the I^{dc} values are such that the corresponding dc-driven resonance frequencies f_0^{dc} fall within the locking range of f_{inj}. Furthermore, our simulations indicate that when the dc-driven precession frequency locks to the external rf, the frequencies and orbits are correlated such that high f_{inj} drives small orbits while low f_{inj} drives large orbits (also the trend for dc-only driven PS precession). Therefore, the MR drop (with respect to the AP state level) in this region is a direct consequence of the expansion of the precessional orbit that occurs when the dc-driven precession locks to a lower f_{inj} drive frequency corresponding to a larger orbit. As will be shown below, the boundary between regions E and G appearing on the map as a sharp contrast when increasing f_{inj} at a fixed I^{dc} represents the frequency locking boundary.

The scattered gray points in Fig. 5(b) appearing at $I^{dc}>I_c$ for $f_{inj}\sim 3$ GHz, correspond to sustained high amplitude MR oscillations that have not switched after the 20 ns simulation window. Note the higher density of these scattered points for injected frequencies near 3 GHz and $I^{dc}>I_c$. In this region of the diagram, the instability boundary for precessional dynamics (limit of lowest frequency stable orbits) intersects with the frequency locking boundary. In this limit, as will be shown in more detail, the occurrence of frequency locking (before the switching event) can fix the orbit radius (which would naturally increase with increasing I^{dc} in absence I^{rf}) as I^{dc} increases over a small range. This effect can extend the stability range of the dynamics to higher currents.

In Fig. 6 we study the behavior at $T=0$ of the Fourier transform spectra of M_y and the precessional orbits for the case of a fixed $I^{dc}\sim 1$ mA and a fixed amplitude rf excitation of varying frequency f_{inj}. At this I^{dc} level, f_0^{dc} is near 4 GHz. In part (a) we overlap the spectra for the cases with f_{inj} varying from 3.0 to 3.7 GHz. However, only the f_{inj} component is visible on the scale of this figure. We show in part (b) some of these spectra plotted on an expanded scale in order to show the evolution of the dc-driven component as f_{inj} is increased in a range close to f_0^{dc}. As the detuning range drops, the component at the injected frequency grows and the inter-

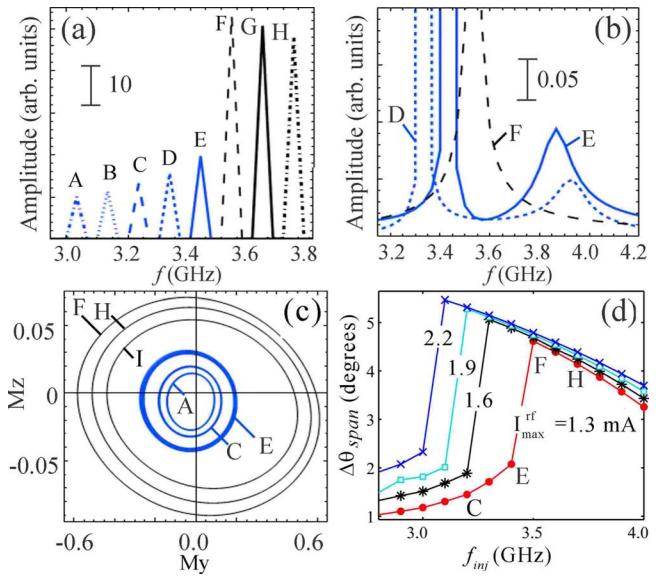

FIG. 6. (Color online) (a) Overlap of the Fourier transform spectra of M_y for I^{rf}_{max}=1.3 mA and f_{inj} varying from 3.0 to 3.7 GHz. (b) Selected spectra from part (a) and plotted with amplitude scale that allows observation of the evolution of the weaker frequency components as f_{inj} is varied. (c) (M_y,M_z) plane precessional orbits corresponding to selected cases from part (a). (d) Out-of-plane angle spanned by the FL magnetization trajectory (in a 20 ns time window) as a function of increasing f_{inj} for several I^{rf} amplitudes. All data obtained through macrospin simulations.

mode interactions make the frequency pulling effects more visible on this time scale. This behavior, with the external rf "pulling" the frequency toward its own frequency ultimately leads to a shift in f_0^{dc} to lower frequencies [see D and E in Fig. 6(b)]. This effect also generates an expansion of the precessional orbit as can be seen in Fig. 6(c), showing (M_y,M_z) plane orbits that correspond to selected frequencies from part (a). From these figures note that both the frequency shift and the orbital expansion are inversely proportional to the detuning range in this regime. Therefore, for orbits A–E we observe an expansion as f_{inj} increases toward (yet below) the locking range.

Frequency locking is obtained for $f_{inj}\sim 3.5$ GHz and above, for which there is a significant increase in the amplitude of the component at f_{inj}, while all other frequency components disappear. The abrupt increase in the amplitude of the spectral component at f_{inj} between E and F in Fig. 6(a) as well as the drop in MR between E and G in Fig. 5(b) suggests that this sudden change in behavior marks the boundary between *partial* frequency locking and frequency locking. In terms of the orbits, this boundary coincides with a significant and abrupt expansion of the precessional orbit (E and F in Fig. 6(c). This expansion is consistent with the fact that the dc-driven precessional frequency locks to a lower injected frequency (3.5 GHz) that drives a larger orbit. Higher f_{inj}, still in the locking range, leads to a gradual *shrinking* (in the frequency locking range, higher frequencies drive smaller orbits) of the orbits [F, H, I in Fig. 6(c)], while the spectra show a decrease in the amplitude at the injected frequency.

Note that the orbits corresponding to single frequency locked spectra exhibit sharp orbits with a narrower spatial spread (F, H, I) in comparison to orbits obtained with f_{inj} outside the locking range where the multiple frequency spectral components are enhanced, and especially in the vicinity of locking (E) where frequency pulling effects are strongest.

Figure 6(d) shows an alternative visualization of this behavior where we plot the out-of-plane angle spanned by the FL magnetization trajectory (in a 20 ns time window) as a function of f_{inj} and for several values of rf peak current amplitude I^{rf}_{max}. This angle is defined as $\Delta\theta_{span}=(\theta_{max}-\theta_{min})/2$. The analogously defined in-plane $\Delta\phi_{span}$ (not shown here) exhibits similar behavior with a larger amplitude. These angles are a measure of the radius of the precessional orbit. Focusing on the I^{rf}_{max}=1.3 mA case, we confirm an abrupt increase in $\Delta\theta_{span}$ as f_{inj} increases above 3.5 GHz followed by a gradual reduction of this angle for higher f_{inj} below 4 GHz.

The effects of varying the amplitude of the injected rf current are also considered in Fig. 6(d). The curves reveal that for higher rf amplitude, full frequency locking occurs at injected frequencies that are further away from f_0^{dc} ($\sim$4 GHz) as is expected. Note also that *only* in the frequency locking region, the angles $\Delta\theta_{span}$ coincide for the various rf amplitudes shown (only these sections of the curves overlap). Similar behavior (not shown here) is obtained for $\Delta\phi_{span}$. Therefore, it appears that the dynamics in the frequency locking regime is determined *only* by the external driving frequency (and not by the rf current amplitude).

Furthermore, for f_{inj} just below the locking range the orbits are found to expand. These expansions appear to be a consequence of frequency pulling effects that occur in the same frequency range. This assertion is substantiated by the fact that the behavior of the orbital expansions follows that of the pulling-induced frequency shifts. That is, both effects are inversely proportional to the detuning range yet proportional to the rf current amplitude. The latter can be seen by the offset in $\Delta\theta_{span}$ observed for f_{inj} below 3.5 GHz and obtained with different I^{rf} amplitudes.

Numerical experiments simulating the behavior of the system when the frequency locking boundary is crossed by fixing f_{inj} and ramping I^{dc} (as in the experiment) were also performed. Results are shown in Fig. 7 where we plot the evolution of the in-plane and out-of-plane spanned angles $\Delta\phi_{span}$ and $\Delta\theta_{span}$ for increasing I^{dc} with I^{rf} of fixed frequency and amplitude (f_{inj}=3.3 GHz). In agreement with previous observations, an abrupt expansion of these angles is observed as I^{dc} reaches I3 (1.17 mA), such that f_0^{dc} and f_{inj} are close enough for the precession to effectively frequency lock to the 3.3 GHz external rf. Note that for higher values of I^{dc}, the angles no longer expand significantly, while the precession remains locked to the external rf. The expansion of the in-plane angle $\Delta\phi_{span}$ from $\sim$10° to 40° (as shown in Fig. 7) is in rough agreement with our preliminary estimation, based on the experimentally measured power in the first and second harmonics, and resulting in an expansion of the precessional angle from 10° to 30° degrees.

The time and frequency behaviors of M_y at several values of I^{dc} increasing from I1 (1.11 mA) to I6 (1.35 mA) without I^{rf} [(a) and (b)] and with I^{rf} [(c) and (d)] can be seen in Fig. 8. Part (a) shows the development and growth of sustained

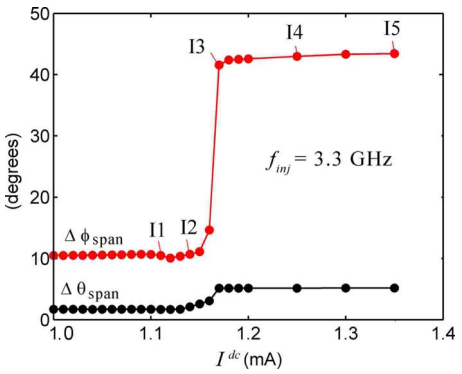

FIG. 7. (Color online) Out-of-plane ($\Delta\theta_{\text{span}}$) and in-plane ($\Delta\phi_{\text{span}}$) angles spanned by the FL magnetization trajectory (in a 20 ns time window) as a function of increasing I^{dc} and obtained through macrospin simulations.

oscillations in M_y as I^{dc} is stepped to higher levels (I1–I6). The corresponding Fourier transforms (calculated for a time window between 20 and 40 ns) are shown in part (b) for cases I1–I6. The peaks have been cropped in order to enhance the visibility of the lower amplitude frequency components. From Figs. 8(a) and 8(b) we confirm that the precessional orbit expands as the corresponding frequencies drop. Figures 8(c) and 8(d) show analogous results obtained by adding a fixed amplitude/frequency (f_{inj}=3.3 GHz) rf current to I^{dc} (for several values, ranging from 1.11 to 1.35 mA). For the low dc current cases I1 (1.11 mA) and I2 (1.14 mA) (dashed), just above the instability threshold, the dc-driven resonance near 4 GHz develops and increases with current [see Fig. 8(d)].

The nonlinearity of the system leads to beating between f_0^{dc} and f_{inj} [see Fig. 8(c)]. For these cases, in frequency domain we find components at the dc-driven frequency f_0^{dc} =4 GHz and at f_{inj}=3.3 GHz, as well as intermodulation products. The latter are expected at frequencies equal to all combinations of the sums and differences of the harmonics and fundamentals of f_0^{dc} and f_{inj}. The strongest components arise at $f_0^{\text{dc}}-f_{\text{inj}}\sim 0.7$ GHz and $f_0^{\text{dc}}+f_{\text{inj}}\sim 7.3$, as well as at $2f_0^{\text{dc}}-f_{\text{inj}}\sim 4.7$ and $2f_{\text{inj}}-f_0^{\text{dc}}\sim 2.6$. As I^{dc} increases from I1 to I2, the detuning separation (between f_0^{dc} and f_{inj}) diminishes while all existing frequency components (fundamental as well as higher order components) grow. However, when I^{dc} is high enough (I3–I6) for f_0^{dc} to be within the locking range of f_{inj}, we observe a substantial increase in the frequency component at f_{inj} while all other frequency components disappear. Note that in this *full* frequency locking range, the amplitude of the M_y oscillations [Fig. 8(c), parts I3–I6] and the corresponding peak frequencies [Fig. 8(d), parts I3–I6] no longer change with I^{dc}. Also note that the M_y oscillation amplitude for case I6 in absence of I^{rf} [Fig. 8(a)] is larger (and at lower frequency [Fig. 8(b)]) than the amplitude at the same current when locked to a rf of higher frequency.

To understand how the rf affects the switching boundary, recall that as the I^{dc} is ramped toward the switching value, the corresponding resonance frequency drops toward $(f_0^{\text{dc}})^{\text{min}}$. If the injected current additionally has a rf component with frequency f_{inj} just below $(f_0^{\text{dc}})^{\text{min}}$, then frequency pulling will open the orbit (f_{inj} pulls toward a lower frequency) as I^{dc}

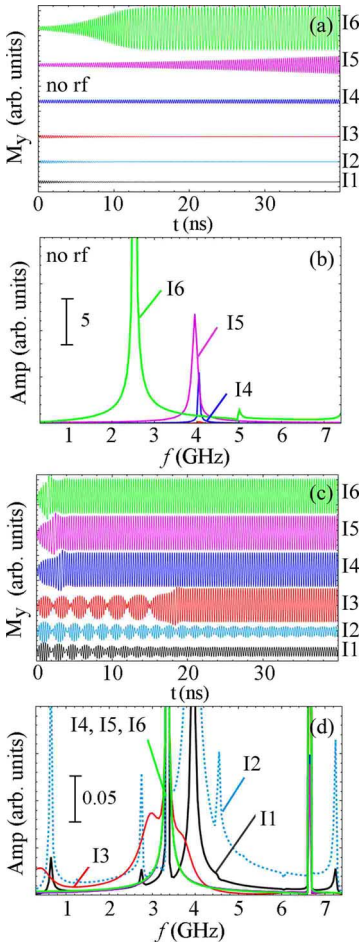

FIG. 8. (Color online) (a) Time evolution of M_y for I^{dc} =1.11 mA (I1), 1.14 mA (I2), 1.17 mA (I3), 1.23 mA (I4), 1.25 mA (I5), 1.35 mA (I6), and I^{rf}=0. (b) Amplitude of Fourier transform of M_y for cases I1–I6. (c) Time evolution of M_y for $I^{\text{rf}}+I^{\text{dc}}$ with f_{inj} =3.3 GHz and I^{dc} varying from I1–I6. (d) Amplitude of Fourier transform of M_y for cases I1–I6, including I^{rf}. The curves in (a) and (c) are vertically offset for clarity.

approaches I_c. This pull drives the system toward f_{inj}, however, since $f_{\text{inj}}<(f_0^{\text{dc}})^{\text{min}}$, there is no stable orbit corresponding to f_{inj}, thus frequency locking does not occur and switching at a reduced I_c is observed. This effect occurs at lower I^{dc} (corresponding to higher f_0^{dc}) values for higher f_{inj} in this range and this may be the origin of the consistent decrease in I_c obtained as f_{inj} increases in the range below $(f_0^{\text{dc}})^{\text{min}}$.

In contrast, for $f_{\text{inj}}\gtrsim(f_0^{\text{dc}})^{\text{min}}$, frequency locking occurs for I^{dc} near the switching boundary, stabilizing the orbit and increasing I_c. As long as the precessional frequency is locked to f_{inj}, the orbit does not expand as I^{dc} increases. Therefore, switching does not occur until I^{dc} is sufficiently high and the corresponding f_0^{dc} is far enough from f_{inj} for the system to unlock and allow the magnetization to switch. For higher frequencies, such that f_{inj} does not remain locked as I^{dc} approaches I_c, there are no expected effects (of this type) of the rf on I_c, as is the case for even higher injected frequencies $f_{\text{inj}}>(f_0^{\text{dc}})^{\text{max}}$ for which no frequency locking occurs.

V. CONCLUSIONS

In conclusion, we demonstrate that rf currents tuned to the frequency range of the dc-driven magnetization precession frequency range can significantly alter the dc-driven PS and switching modes. Based on frequency domain measurements and macrospin simulations that well describe our experimental data, we explain the origin of the rf-driven effects through an understanding of the precessional orbits and frequencies and the subsequent influence on the dc critical switching boundary. This mechanism for controlling I_c by additionally injecting rf currents with frequencies in the (f_0^{dc}) range may be of technological interest for the design of STT devices.

ACKNOWLEDGMENTS

We acknowledge helpful communications with J. Sun and K. Ito and thank I. Krivorotov for providing the macrospin simulation code.

*sylvia.florez@hitachigst.com

[1] L. Berger, Phys. Rev. B **54**, 9353 (1996).
[2] J. Slonczewski, J. Magn. Magn. Mater. **195**, 261 (1999).
[3] S. I. Kiselev, J. C. Sankey, I. N. Krivorotov, N. C. Emley, R. J. Schoelkopf, R. A. Buhrman, and D. C. Ralph, Nature (London) **425**, 380 (2003).
[4] T. Devolder, P. Crozat, C. Chappert, J. Miltat, A. Tulapurkar, Y. Suzuki, and K. Yagami, Phys. Rev. B **71**, 184401 (2005).
[5] J. Z. Sun, Phys. Rev. B **62**, 570 (2000).
[6] M. D. Stiles and J. Miltat, *Spin Dynamics in Magnetic Structures III* (Springer, Berlin, 2006).
[7] O. Ozatay *et al.*, Nature Mater. **7**, 567 (2008).
[8] W. H. Rippard, M. R. Pufall, S. Kaka, T. J. Silva, S. E. Russek, and J. A. Katine, Phys. Rev. Lett. **95**, 067203 (2005).
[9] A. A. Tulapurkar, T. Devolder, K. Yagami, P. Crozat, C. Chappert, A. Fukushima, and Y. Suzuki, Nature (London) **438**, 339 (2005).
[10] J. C. Sankey, P. M. Braganca, A. G. F. Garcia, I. N. Krivorotov, R. A. Buhrman, and D. C. Ralph, Phys. Rev. Lett. **96**, 227601 (2006).
[11] S. H. Florez, J. A. Katine, M. Carey, L. Folks, and B. D. Terris, J. Appl. Phys. **103**, 07A708 (2008).
[12] K. J. Lee, A. Deac, O. Redon, J. Nozieres, and B. Dieny, Nature Mater. **3**, 877 (2004).
[13] J.-G. Zhu, X. Zhu, and Y. Tang, IEEE Trans. Magn. **44**, 125 (2008).
[14] C. Thirion, W. Wernsdorfer, and D. Mailly, Nature Mater. **2**, 524 (2003).
[15] A. Pivosky, M. Rosenblum, and J. Kurths, *Synchronization* (Cambridge University Press, Cambridge, 2001).